Continuous Matrix Product Operator Approach to Finite Temperature Quantum States

Wei Tang,[1] Hong-Hao Tu,[2,*] and Lei Wang[3,4,†]
[1]International Center for Quantum Materials, School of Physics, Peking University, Beijing 100871, China
[2]Institute of Theoretical Physics, Technische Universität Dresden, 01062 Dresden, Germany
[3]Beijing National Lab for Condensed Matter Physics and Institute of Physics, Chinese Academy of Sciences, Beijing 100190, China
[4]Songshan Lake Materials Laboratory, Dongguan, Guangdong 523808, China

(Received 8 May 2020; accepted 16 September 2020; published 23 October 2020)

We present an algorithm for studying quantum systems at finite temperature using continuous matrix product operator representation. The approach handles both short-range and long-range interactions in the thermodynamic limit without incurring any time discretization error. Moreover, the approach provides direct access to physical observables including the specific heat, local susceptibility, and local spectral functions. After verifying the method using the prototypical quantum *XXZ* chains, we apply it to quantum Ising models with power-law decaying interactions and on the infinite cylinder, respectively. The approach offers predictions that are relevant to experiments in quantum simulators and the nuclear magnetic resonance spin-lattice relaxation rate.

DOI: 10.1103/PhysRevLett.125.170604

Introduction.—Despite being used as a standard method for studying ground states of low-dimensional quantum systems [1–4], tensor network approaches to thermal states are still under continuous development [5–22]. Ideally, for translationally invariant systems we would like to have a method that directly works in the thermodynamical limit, handles long-range interactions and two-dimensional geometry well, has no imaginary-time discretization error, and even better, provides access to dynamical properties such as finite temperature spectral functions.

The existing approaches have made a trade-off in meeting either this or that from the wish list. The difficulties are that, although the partition function of a quantum system could be formally treated as a tensor network defined in a one-dimensional-higher space-time manifold with an imaginary-time direction, the tensor network has a periodic boundary condition in the time direction with a periodicity given by the inverse temperature $\beta = 1/T$. Moreover, the tensor network is highly anisotropic as it is continuous along the imaginary-time direction. These features made it nontrivial to transferring those highly successful tensor network approaches developed for the ground-state calculation.

In this work, we present an approach to study quantum systems at finite temperature centered around the concept of continuous matrix product operators (cMPOs). The approach works in the thermodynamic limit and the continuous-time limit simultaneously. Besides the obvious advantages of eliminating the finite-size and time-discretization errors, the approach directly applies to systems with long-range interactions by virtue of the MPO representation. Moreover, a distinguishing feature of the present approach is that it offers ways to straightforwardly measure physical observables such as unequal-time correlation functions and dynamical responses at finite temperature. In analogy to the density matrix renormalization group (DMRG) [3], quasi-one-dimensional systems with a cylindrical geometry are also within the scope of the cMPO method, which opens a way to study statistical and dynamical properties of two-dimensional quantum systems at finite temperature.

The present approach stems from a compact MPO representation of the evolution operator for time evolving long-range interacting systems [23]. Despite being simple and elegant, the original MPO representation has an intrinsic time-discretization error, which was shown to be not accurate enough for practical calculations [23,24]. We show that one can eliminate the time discretization error by formally taking the continuous-time limit in the tensor network algorithm in the same spirit as the continuous-time quantum Monte Carlo (QMC) approaches [25,26]. A tensor network formed by cMPOs appears naturally in the continuous-time limit. To contract such tensor network, one encounters the continuous matrix product state (cMPS) [27] as the dominant eigenvector of the cMPO. Having such cMPS along the imaginary-time direction of finite temperature quantum systems has been anticipated in Refs. [28,29], but its implications for practical calculations have been largely unexplored.

cMPO formulation.—There is a general recipe to construct the MPO representation of a Hamiltonian H, including those with long-range interactions [30–33]. Building on such representation, one can also construct an accurate MPO representation for the evolution operator $e^{-\epsilon H}$ provided the time step ϵ is sufficiently small [23,34]. Since we will consider the limit of $\epsilon \to 0$, we shall not be concerned

about the time discretization error and write the evolution operator as a translationally invariant MPO, $e^{-\epsilon H} = \cdots$ 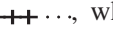 $\cdots$, where the vertical legs of the MPO tensor represent the d-dimensional physical Hilbert space at each site, and the horizontal legs carry D-dimensional virtual degrees of freedom. When viewing the left and right legs of the MPO tensor as matrix indices, the tensor at each site takes the same form [23]

$$+_{ij} = \begin{pmatrix} \mathbb{1} + \epsilon Q & \sqrt{\epsilon}\boldsymbol{L} \\ \sqrt{\epsilon}\boldsymbol{R} & \boldsymbol{P} \end{pmatrix}_{ij}, \tag{1}$$

where the subscripts $i, j \in [1, D]$ are virtual indices and each matrix entry $+_{ij}$ is an operator acting on the d-dimensional physical Hilbert space. In terms of the virtual indices, the compact notation in Eq. (1) denotes that $\mathbb{1}$ (identity operator) and Q are scalars, $\boldsymbol{L}$ ($\boldsymbol{R}$) is a $(D-1)$-dimensional row (column) vector, and $\boldsymbol{P}$ is a $(D-1)$-dimensional square matrix. Q is related to the local terms in the Hamiltonian, $\boldsymbol{L}$, $\boldsymbol{R}$ contain interaction to neighboring sites, and $\boldsymbol{P}$ is responsible for long-range interactions. The concrete form of Q, $\boldsymbol{L}$, $\boldsymbol{R}$, $\boldsymbol{P}$ can be read out from the MPO representation of the Hamiltonian, examples of which are given in Ref. [35].

In this framework, the partition function at finite temperature is written as

$$Z = \mathrm{Tr}(e^{-\beta H}) = \mathrm{Tr}[(\cdots \text{} \cdots)^{\beta/\epsilon}], \tag{2}$$

where the β/ϵth power of the MPO (representing the infinitesimal evolution operator $e^{-\epsilon H}$) indeed recovers $e^{-\beta H}$ and the trace connects the remaining physical indices pointing upwards and downwards. The partition function Eq. (2) has an explicit tensor network representation formed by stacking the local tensors defined in Eq. (1). In the thermodynamic limit $L \to \infty$, the tensor network has an infinite cylinder geometry as shown in Fig. 1(a).

We highlight the central object of the present approach in Fig. 1(a), the transfer matrix $\mathbb{T}$, which is an MPO with horizontal open legs along the spatial direction. In the limit $\epsilon \to 0$, $\mathbb{T}$ becomes a cMPO with "length" β in the periodic imaginary-time direction. In the thermodynamic limit, the dominant eigenvalue of $\mathbb{T}$, which we denote by $\lambda_{\max}$ and assume to be unique [51], completely determines the partition function, $Z = \lim_{L\to\infty} \lambda_{\max}^L$ [5,6]. The left and right eigenvectors associated with $\lambda_{\max}$ are respectively denoted by $\langle l|$ and $|r\rangle$ and satisfy

$$\mathbb{T}|r\rangle = \lambda_{\max}|r\rangle, \qquad \langle l|\mathbb{T} = \langle l|\lambda_{\max}. \tag{3}$$

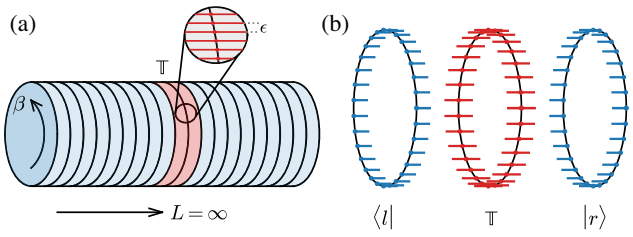

FIG. 1. (a) The partition function as a space-time tensor network living on an infinite cylinder. (b) The transfer matrix $\mathbb{T}$ as a cMPO and its left and right dominant eigenvectors as two cMPSs.

Under the tensor network framework, we approximate $\langle l|$ and $|r\rangle$ by using two MPSs with finite bond dimensions [see Fig. 1(b)]. The MPSs are taken to be uniform, i.e., translationally invariant along the imaginary-time direction. For instance, the MPS for $|r\rangle$ is defined through a local tensor

$$\dashv_i = \begin{pmatrix} \mathbb{1}_\dashv + \epsilon Q_\dashv \\ \sqrt{\epsilon}\boldsymbol{R}_\dashv \end{pmatrix}_i, \tag{4}$$

where $i \in [1, D]$ is the index of the horizontal tensor legs in the spatial direction. The MPS has bond dimension χ along the imaginary-time direction. Hence, $\mathbb{1}_\dashv$ is the χ-dimensional identity matrix, $Q_\dashv$ is a $\chi \times \chi$ matrix, and $\boldsymbol{R}_\dashv$ is a $(D-1)$-dimensional column vector, each entry of which is a $\chi \times \chi$ matrix. The local tensor $\vdash_i$ for defining $\langle l|$ has the same structure as Eq. (4), which contains $\mathbb{1}_\vdash$, $Q_\vdash$, and $\boldsymbol{R}_\vdash$. In the limit $\epsilon \to 0$, both the left and right MPSs reduce to cMPS. Compared to the original formulation of cMPSs in the continuous space [27], the imaginary-time direction is continuous and periodic in the present setting.

Given the left and right cMPSs, the dominant eigenvalue of $\mathbb{T}$ can be estimated from the quotient $\lambda_{\max} = \langle l|\mathbb{T}|r\rangle / \langle l|r\rangle$. First, to compute the overlap $\langle l|r\rangle$ in the denominator, one can form a (temporal) transfer matrix $\vdash\!\dashv$ along the imaginary-time direction, where the connected leg sums over the horizontal indices of two cMPS local tensors. To the leading order of ϵ, one has [27]

$$\vdash\!\dashv = \mathbb{1}_\vdash \otimes \mathbb{1}_\dashv + \epsilon \underbrace{(Q_\vdash \otimes \mathbb{1}_\dashv + \mathbb{1}_\vdash \otimes Q_\dashv + \boldsymbol{R}_\vdash \otimes \boldsymbol{R}_\dashv)}_{-K_{\vdash\dashv}}, \tag{5}$$

where $\boldsymbol{R}_\vdash \otimes \boldsymbol{R}_\dashv$ already assumed summation over the horizontal index, and $K_{\vdash\dashv}$ is a $\chi^2 \times \chi^2$ matrix by combining two legs upward and downward. Given Eq. (5), the overlap can be evaluated in the continuous-time limit as [27]

$$\langle l|r\rangle = \lim_{\epsilon\to 0} \mathrm{Tr}\left(\vdash\!\dashv^{\beta/\epsilon}\right) = \mathrm{Tr}\, e^{-\beta K_{\vdash\dashv}}. \tag{6}$$

Moreover, applying a cMPO to a cMPS yields another cMPS, as long as the first-order terms in ϵ are retained. Thus, $\mathbb{T}|r\rangle$ can be viewed as a cMPS defined via a local tensor

$$\text{⊢⊣}_i = \begin{pmatrix} \mathbb{1}_+ \otimes \mathbb{1}_\dashv + \epsilon(\mathbb{1}_+ \otimes Q_\dashv + Q_+ \otimes \mathbb{1}_\dashv + L_+ \otimes R_\dashv) \\ \sqrt{\epsilon}(R_+ \otimes \mathbb{1}_\dashv + P_+ \otimes R_\dashv) \end{pmatrix}_i, \tag{7}$$

where the subscript $+$ refers to tensors from $\mathbb{T}$ [see Eq. (1)]. Then, the overlap $\langle l|$ and $\mathbb{T}|r\rangle$ involves another (temporal) transfer matrix $\text{⊢⊣} = \mathbb{1}_\vdash \otimes \mathbb{1}_+ \otimes \mathbb{1}_\dashv - \epsilon K_{\text{⊢⊣}}$ defined in a similar way as Eq. (5), with $K_{\text{⊢⊣}}$ being a $\chi^2 d \times \chi^2 d$ matrix. Given this, the expectation reads

$$\langle l|\mathbb{T}|r\rangle = \lim_{\epsilon\to 0} \mathrm{Tr}\left(\text{⊢⊣}^{\beta/\epsilon}\right) = \mathrm{Tr}\, e^{-\beta K_{\text{⊢⊣}}}. \tag{8}$$

It is worth emphasizing that taking the $\epsilon \to 0$ limit in Eqs. (6) and (8) has eliminated the time discretization error.

By combining Eqs. (6) and (8), the free-energy density $f = -\ln Z/(\beta L)$ takes a simple form:

$$f = -\frac{1}{\beta}\left(\ln \mathrm{Tr}\, e^{-\beta K_{\text{⊢⊣}}} - \ln \mathrm{Tr}\, e^{-\beta K_{\text{⊢}}}\right). \tag{9}$$

In the cases where the spatial transfer matrix $\mathbb{T}$ is Hermitian, one has $|l\rangle = |r\rangle$. One can directly minimize Eq. (9) with respect to the cMPS tensors according to the variational free-energy principle. This calculation is equivalent to optimizing a periodic uniform cMPS as the dominant eigenvector of a Hermitian cMPO. Without loss of generality, notice that the temporal transfer matrices ⊢ and ⊢⊣ can always be gauged to be Hermitian, so are $K_{\text{⊢}}$ and $K_{\text{⊢⊣}}$ [52]. The matrix exponential can be evaluated with eigendecomposition with a computational cost of $\mathcal{O}(\chi^6)$. It is nevertheless possible to further reduce the complexity by using an approximation scheme to compute the trace exponentials. In particular, at the zero-temperature limit $\beta \to \infty$, the trace exponentials are dominated by the smallest eigenvalues of $K_{\text{⊢⊣}}$ and $K_{\text{⊢}}$. In this case, the scaling reduces to $\mathcal{O}(\chi^3)$ if one employs a dominant eigensolver for $K_{\text{⊢⊣}}$ and $K_{\text{⊢}}$.

In more general cases, the spatial transfer matrix $\mathbb{T}$ is non-Hermitian. Under such a situation, we employ the power method to find the cMPS approximations of the dominant eigenvectors $\langle l|$ and $|r\rangle$. In each step of the power projection, we apply the transfer matrix $\mathbb{T}$ to an initial cMPS with bond dimension χ and obtain a cMPS built by ⊢⊣ with an enlarged bond dimension χd. We then compress it back to bond dimension χ by variationally maximizing the fidelity between the target cMPS $|\psi\rangle$ and $\mathbb{T}|r\rangle$

$$\mathcal{F} = \langle\psi|\mathbb{T}|r\rangle/\sqrt{\langle\psi|\psi\rangle}. \tag{10}$$

Calculations involved in this objective function are similar to those of the free-energy density in Eq. (9). To optimize these quantities, we perform gradient-based variational optimizations using the limited-memory Broyden-Fletcher-Goldfarb-Shanno (L-BFGS) quasi-Newton algorithm, where we employ the differentiable programming approach [53] to compute the gradient with respect to the cMPS tensors conveniently. The explicit derivation of the gradient and the initialization strategies of the variational optimization are given in Ref. [35].

After obtaining the boundary cMPS approximations for the dominant eigenvectors of the spatial transfer matrix $\mathbb{T}$, one can compute a number of physical observables. First, defining $O = \mathbb{1}_\vdash \otimes O_i \otimes \mathbb{1}_\dashv$ allows one to calculate the thermal average of local operators as

$$\langle O_i\rangle = \mathrm{Tr}\left(e^{-\beta K_{\text{⊢⊣}}} O\right) / \mathrm{Tr}\left(e^{-\beta K_{\text{⊢⊣}}}\right), \tag{11}$$

where, curiously, $K_{\text{⊢⊣}}$ acts as an "effective Hamiltonian" and $e^{-\beta K_{\text{⊢⊣}}}$ plays the role of the single-site reduced density matrix after leaving the physical indices untraced [54]. Having access to the temporal transfer matrix ⊢⊣ also allows computing the local two-time correlation function conveniently [55]

$$\langle A_i(\tau)B_i\rangle = \mathrm{Tr}\left(e^{-(\beta-\tau)K_{\text{⊢⊣}}} A e^{-\tau K_{\text{⊢⊣}}} B\right) / \mathrm{Tr}\left(e^{-\beta K_{\text{⊢⊣}}}\right). \tag{12}$$

An example of this is the spin-spin correlation function $\chi(\tau) \equiv \langle S_i^z(\tau) S_i^z\rangle$. The corresponding Matsubara frequency susceptibility $\chi(i\omega)$ is computed using the eigenvalue decomposition of the effective Hamiltonian $K_{\text{⊢⊣}}$. Crucially, one can directly perform analytic continuation to real frequencies to obtain the dynamical susceptibility $\chi''(\omega) \equiv \mathrm{Im}\chi(i\omega \to \omega + i0^+)$ given the spectral representation. Moreover, the local spectral function $S(\omega) = 2\chi''(\omega)/(1 - e^{-\beta\omega})$ follows according to the fluctuation-dissipation theorem [36]. The details on the computation of these dynamical quantities in the cMPO framework are given in Ref. [35].

Moreover, the energy density and the specific heat can be directly computed by taking the explicit derivative of the free-energy density in Eq. (9) with respect to the inverse temperature [56],

$$e = \langle K_{\text{⊢⊣}}\rangle_{K_{\text{⊢⊣}}} - \langle K_{\text{⊢}}\rangle_{K_{\text{⊢}}}, \tag{13}$$

$$c = \beta^2\left[\left(\langle K_{\text{⊢⊣}}^2\rangle_{K_{\text{⊢⊣}}} - \langle K_{\text{⊢⊣}}\rangle_{K_{\text{⊢⊣}}}^2\right) - \left(\langle K_{\text{⊢}}^2\rangle_{K_{\text{⊢}}} - \langle K_{\text{⊢}}\rangle_{K_{\text{⊢}}}^2\right)\right], \tag{14}$$

where the notations $\langle\cdots\rangle_{K_{\text{⊢}}}$ and $\langle\cdots\rangle_{K_{\text{⊢⊣}}}$ stand for the thermal average over the effective Hamiltonians and $K_{\text{⊢⊣}}$, respectively. Having a direct estimator for the specific heat is more convenient than computing numerical differentiation on a fine scan of temperature. However, one should also be cautioned that the estimators in Eqs. (13) and (14) hold only upon the convergence of the power projection.

The specific heat estimator can be less reliable than numerical differentiation at low temperature since it involves subtraction of large numbers, similar to the case of stochastic series expansion QMC method [57]. Our code implementation is publicly available at Ref. [58].

Results.—As the first application, we consider the quantum spin-1/2 *XXZ* chain

$$H = \sum_{\langle i,j \rangle} (S_i^x S_j^x + S_i^y S_j^y + \Delta S_i^z S_j^z), \tag{15}$$

where Δ is the anisotropy parameter. The model reduces to the quantum *XY* model at $\Delta = 0$ and the Heisenberg model at $\Delta = 1$. In general, the cMPO representation for the quantum *XXZ* chain has $D = 4$ [35]. We note that, when $\Delta \geq 0$, it is possible to perform a basis rotation to bring the cMPO into a Hermitian form which allows a direct variational optimization of Eq. (9). We nevertheless employ the power method for its generality. The bond dimension of the boundary cMPS is fixed to be $\chi = 20$ in this study.

Figure 2(a) shows the specific heat of the quantum *XXZ* chain at various Δ. For both *XY* and Heisenberg cases, the specific heat vanishes linearly with respect to T, which is in agreement with conformal field theory predictions [59,60]. Figure 2(b) shows that the imaginary-time correlator reaches higher values in the large time limit with increasing of Δ, indicating the development of long-range correlations along the imaginary-time direction. As a consequence, the local susceptibility $T\chi_{\mathrm{loc}} = (1/\beta)\int_0^\beta d\tau \chi(\tau)$ indicates the local moment in the low-temperature limit as shown in Fig. 2(c). In the *XY* case, all of the physical quantities computed with the cMPO method are in excellent agreement with the exact results [35].

Furthermore, Fig. 2(d) shows the local spectral function $S(\omega)$ calculated directly in the real frequency using the spectral decomposition of $K_{\mapsto\mapsto}$. Although dynamical properties are more sensitive to the convergence of the boundary cMPS than thermodynamic quantities, the comparison to the exact results in the *XY* limit [61] shows encouraging agreement, especially in the low-frequency region. In particular, the zero frequency value of the local spectral function is related to the nuclear magnetic resonance (NMR) spin-lattice relaxation rate measured in experiments [62] which indicates the strength of low-energy fluctuations. There have been extensive efforts in studying this quantity both analytically and numerically [63–69]. At high frequencies, the multipeak structure and the inconsistency with the exact solution are attributed to the finiteness of the "effective Hamiltonian." The high-frequency results can be improved by increasing the bond dimension. By far, two predominant numerical approaches are based on analytic continuation of imaginary time correlation functions [37,38,70] and Fourier transform of the extrapolated real-time data [71–74]. The cMPO approach offers a way to compute finite temperature spectral functions without getting into the tricky business of analytic continuation of imaginary-time data or prediction of real-time series. Moreover, the cMPO approach applies more broadly to frustrated systems with long-range interactions, which means it is applicable to quasi-one-dimensional systems with a cylindrical geometry, in a similar spirit as the applications of the DMRG in this geometry [3]. Further investigations are needed to fully explore this direction and make an extensive and quantitative comparison between various approaches. We remark that, as a bottom line, one can always only deal with the imaginary-time data [75,76] and employ recent advances in analytic continuation to impose prior knowledge in the spectrum [77,78].

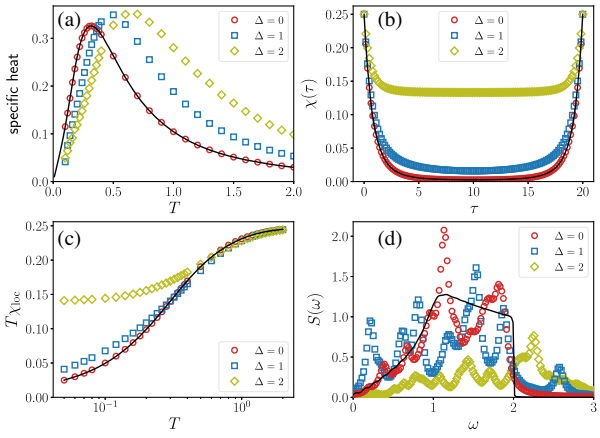

FIG. 2. (a) The specific heat computed with Eq. (14); (b) local unequal time spin correlation function at $\beta = 20$; (c) the local susceptibility; (d) the local spectral function of the *XXZ* chain with various anisotropies. The solid black lines are the exact results in the *XY* limit.

Finally, we consider the transverse field Ising model with long-range interactions defined by the following Hamiltonian:

$$H = -\sum_{i<j} J_{i,j} Z_i Z_j - \Gamma \sum_i X_i, \tag{16}$$

where X and Z are Pauli matrices. First, assuming the spins are arranged in a one-dimensional chain and the coupling follows a power-law decaying interaction $J_{i,j} = J/|j-i|^\alpha$, the Hamiltonian is relevant to trapped ions and Rydberg atom quantum simulators realized experimentally [79–82]. Although the power α is tunable in a range, we focus here on the case of inverse-square interaction, i.e., $\alpha = 2$, where the model exhibits a Kosterlitz-Thouless transition as the temperature changes [83,84]. When $J = 1$, in the ground state the model exhibit a quantum multicritical point at $\Gamma_c \approx 2.5236$ [85,86]. To handle the long-range interaction, we follow Ref. [32] to represent the power-law decaying interaction as a sum of exponentials [35]. Figure 3(a) shows the local susceptibility calculated in the inverse-square Ising chain. In the ordered phase, the local

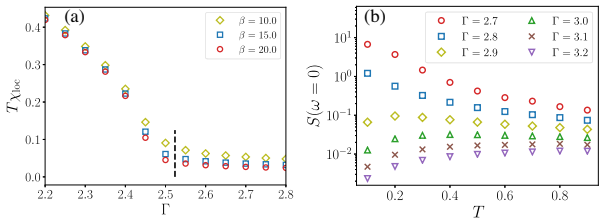

FIG. 3. (a) The local susceptibility of the inverse-square Ising chain with a transverse field. The bond dimension of the cMPS is $\chi = 20$. The vertical dashed line marks the quantum multicritical point at $\Gamma_c \approx 2.5236$ [85,86]. (b) The zero frequency local spectral function of the transverse field Ising model on a cylinder with width $W = 4$.

susceptibility remains a finite value at zero temperature, while it vanishes in the disordered phase. By calculating $T\chi_{\rm loc}$ for different transverse fields and temperatures, we find our results consistent with the QMC prediction on the location of the quantum multicritical point [85,86].

Next, we turn to the model in Eq. (16) on a quasi-one-dimensional lattice with cylindrical geometry. Consider an infinitely long cylinder with circumference W. If we impose the helical boundary condition, the Hamiltonian can be regarded as a one-dimensional Ising chain with $J_{i,i+j} = J$ if $j = 1$ or W, and zero otherwise. The bond dimension of the cMPO is $D = W + 1$ [35]. In the two-dimensional limit $W \to \infty$, the transverse field Ising model shows a quantum critical point at $\Gamma_c = 3.04438(2)$ [39,87]. Here we focus on a finite width cylinder $W = 4$ and study the temperature dependence of the zero-frequency local spectral function across the quantum critical point. Figure 3(b) shows that in the ordered phase the spectral function increases when lowering the temperature due to the presence of elastic modes. Meanwhile, the spectral function is suppressed in the quantum disorder phase at the low-temperature limit. Such drastically different behaviors were observed previously in the NMR relaxation rate across the quantum critical point of the quantum Ising chain [88]. Having a numerical probe of the quantity for the quasi-one-dimensional case opens an opportunity to access the spectral information of frustrated magnets and even fermions in two dimensions [89,90].

Summary and discussion.—To summarize, we have put forward an algorithm for studying quantum systems at finite temperature by developing cMPO techniques. This approach works directly in the thermodynamic limit and does not have any time-discretization errors. Moreover, this approach works well for long-range interactions and can compute local dynamical properties. The basics of the present approach is the MPO representation of the evolution operator in the continuous-time limit. For future works, the compression scheme for MPO representation of long-range interacting Hamiltonians [91–93] may be used to obtain more compact cMPOs for thermal state calculations. In the cMPO framework, the effective Hamiltonians $K_{\mapsto}$ and $K_{\mapsto\mapsto}$ play a central role in the computation as well as governing the physics. It would be worth investigating their properties and universal behaviors more closely.

The cMPO representation can also be extended to higher-dimensional tensor networks [35]. Given the contraction algorithm of the partition function in the $1 + 1$ dimensions presented here, one envisions a contraction scheme in $2 + 1$ dimensions along the line of Refs. [94–96], which would directly provide thermal properties of infinite two-dimensional systems other than the cylinders considered here. However, this algorithm also features nested variational optimization and projection with higher computational costs, which deserve further investigation [97].

We thank Tao Xiang, Hai-Jun Liao, Zhi-Yuan Xie, and Wei Li for fruitful discussions. L. W. is supported by the Ministry of Science and Technology of China under the Grants No. 2016YFA0300603 and No. 2016YFA0302400, the National Natural Science Foundation of China under Grant No. 11774398. H.-H. T. is supported by the DFG through project A06 of SFB 1143 (Project-id 247310070).

*hong-hao.tu@tu-dresden.de
†wanglei@iphy.ac.cn

[1] F. Verstraete, V. Murg, and J. I. Cirac, Adv. Phys. **57**, 143 (2008).
[2] U. Schollwöck, Ann. Phys. (Amsterdam) **326**, 96 (2011).
[3] E. M. Stoudenmire and S. R. White, Annu. Rev. Condens. Matter Phys. **3**, 111 (2012).
[4] R. Orús, Nat. Rev. Phys. **1**, 538 (2019).
[5] R. J. Bursill, T. Xiang, and G. A. Gehring, J. Phys. Condens. Matter **8**, L583 (1996).
[6] X. Wang and T. Xiang, Phys. Rev. B **56**, 5061 (1997).
[7] T. Xiang, Phys. Rev. B **58**, 9142 (1998).
[8] N. Shibata, J. Phys. Soc. Jpn. **66**, 2221 (1997).
[9] F. Verstraete, J. J. García-Ripoll, and J. I. Cirac, Phys. Rev. Lett. **93**, 207204 (2004).
[10] M. Zwolak and G. Vidal, Phys. Rev. Lett. **93**, 207205 (2004).
[11] A. E. Feiguin and S. R. White, Phys. Rev. B **72**, 220401(R) (2005).
[12] S. R. White, Phys. Rev. Lett. **102**, 190601 (2009).
[13] E. M. Stoudenmire and S. R. White, New J. Phys. **12**, 055026 (2010).
[14] W. Li, S.-J. Ran, S.-S. Gong, Y. Zhao, B. Xi, F. Ye, and G. Su, Phys. Rev. Lett. **106**, 127202 (2011).
[15] Z. Y. Xie, J. Chen, M. P. Qin, J. W. Zhu, L. P. Yang, and T. Xiang, Phys. Rev. B **86**, 045139 (2012).
[16] P. Czarnik and J. Dziarmaga, Phys. Rev. B **92**, 035152 (2015).
[17] B.-B. Chen, Y. J. Liu, Z. Chen, and W. Li, Phys. Rev. B **95**, 161104(R) (2017).
[18] B.-B. Chen, L. Chen, Z. Chen, W. Li, and A. Weichselbaum, Phys. Rev. X **8**, 031082 (2018).
[19] A. Kshetrimayum, M. Rizzi, J. Eisert, and R. Orús, Phys. Rev. Lett. **122**, 070502 (2019).

[20] C.-M. Chung and U. Schollwöck, arXiv:1910.03329.
[21] J. Chen and E. M. Stoudenmire, Phys. Rev. B **101**, 195119 (2020).
[22] B.-B. Chen, Y. Gao, Y.-B. Guo, Y. Liu, H.-H. Zhao, H.-J. Liao, L. Wang, T. Xiang, W. Li, and Z. Y. Xie, Phys. Rev. B **101**, 220409(R) (2020).
[23] M. P. Zaletel, R. S. K. Mong, C. Karrasch, J. E. Moore, and F. Pollmann, Phys. Rev. B **91**, 165112 (2015).
[24] B. Bruognolo, Z. Zhu, S. R. White, and E. M. Stoudenmire, arXiv:1705.05578.
[25] B. B. Beard and U. J. Wiese, Phys. Rev. Lett. **77**, 5130 (1996).
[26] N. V. Prokof'ev, B. V. Svistunov, and I. S. Tupitsyn, JETP Lett. **64**, 911 (1996).
[27] F. Verstraete and J. I. Cirac, Phys. Rev. Lett. **104**, 190405 (2010).
[28] M. B. Hastings and R. Mahajan, Phys. Rev. A **91**, 032306 (2015).
[29] E. Tirrito, L. Tagliacozzo, M. Lewenstein, and S.-J. Ran, arXiv:1810.08050.
[30] I. P. McCulloch, J. Stat. Mech. (2007) P10014.
[31] G. M. Crosswhite and D. Bacon, Phys. Rev. A **78**, 012356 (2008).
[32] G. M. Crosswhite, A. C. Doherty, and G. Vidal, Phys. Rev. B **78**, 035116 (2008).
[33] F. Fröwis, V. Nebendahl, and W. Dür, Phys. Rev. A **81**, 062337 (2010).
[34] B. Pirvu, V. Murg, J. I. Cirac, and F. Verstraete, New J. Phys. **12**, 025012 (2010).
[35] See Supplemental Material at http://link.aps.org/supplemental/10.1103/PhysRevLett.125.170604 for further details on the cMPO representations and its motivation from the worldline picture, analytical gradient of the objective function, initialization in variational optimizations, computations of dynamical susceptibility and Klein bottle entropy, the exact results for the *XY* chain, and the benchmark in the critical quantum Ising chain, which includes Refs. [33,36–50].
[36] S. Sachdev, *Quantum Phase Transitions*, 2nd ed. (Cambridge University Press, Cambridge, 2011).
[37] M. Jarrell and J. E. Gubernatis, Phys. Rep. **269**, 133 (1996).
[38] A. W. Sandvik, Phys. Rev. B **57**, 10287 (1998).
[39] H. Rieger and N. Kawashima, Eur. Phys. J. B **9**, 233 (1999).
[40] J. Motruk, M. P. Zaletel, R. S. Mong, and F. Pollmann, Phys. Rev. B **93**, 155139 (2016).
[41] B. Vanhecke, L. Vanderstraeten, and F. Verstraete, arXiv:1912.10512.
[42] Y. Zou, A. Milsted, and G. Vidal, Phys. Rev. Lett. **121**, 230402 (2018).
[43] M. Ganahl, J. Rincón, and G. Vidal, Phys. Rev. Lett. **118**, 220402 (2017).
[44] G. Evenbly and G. Vidal, Phys. Rev. B **79**, 144108 (2009).
[45] R. Orus and G. Vidal, Phys. Rev. B **78**, 155117 (2008).
[46] B. Vanhecke, M. Van Damme, J. Haegeman, L. Vanderstraeten, and F. Verstraete, arXiv:2001.11882.
[47] H.-H. Tu, Phys. Rev. Lett. **119**, 261603 (2017).
[48] W. Tang, L. Chen, W. Li, X. C. Xie, H.-H. Tu, and L. Wang, Phys. Rev. B **96**, 115136 (2017).
[49] L. Chen, H.-X. Wang, L. Wang, and W. Li, Phys. Rev. B **96**, 174429 (2017).
[50] W. Tang, X. Xie, L. Wang, and H.-H. Tu, Phys. Rev. B **99**, 115105 (2019).
[51] The degeneracy in the dominant eigenvalue of $\mathbb{T}$ indicates long-range correlations between local operators. This cannot occur at finite temperature for generic one-dimensional quantum systems with local interactions, but may happen in long-range interacting systems.
[52] For example, one way to keep the Hermicity of $K_{\mapsto}$ and $K_{\mapsto\mapsto}$ is to choose the gauge where all matrices in the cMPO are Hermitian, and, meanwhile, fix the matrices in the cMPS to be Hermitian during variational optimizations. In practice, we can avoid the difficulty in choosing the gauge by always manually symmetrizing $K_{\mapsto}$ and $K_{\mapsto\mapsto}$ before diagonalizing them.
[53] H. J. Liao, J. G. Liu, L. Wang, and T. Xiang, Phys. Rev. X **9**, 031041 (2019).
[54] Computing spatially nonlocal correlation function will involve constructing the transfer matrix  and contracting the resulting tensor network approximately.
[55] M. C. Bañuls, M. B. Hastings, F. Verstraete, and J. I. Cirac, Phys. Rev. Lett. **102**, 240603 (2009).
[56] The implicit derivative through the boundary cMPS vanishes at the variational extreme, as a consequence of the Feynman-Hellmann theorem.
[57] A. W. Sandvik, AIP Conf. Proc. **1297**, 135 (2010).
[58] See https://github.com/TensorBFS/cMPO for code implementation in PyTorch.
[59] I. Affleck, Phys. Rev. Lett. **56**, 746 (1986).
[60] H. W. J. Blöte, J. L. Cardy, and M. P. Nightingale, Phys. Rev. Lett. **56**, 742 (1986).
[61] H. B. Cruz and L. L. Goncalves, J. Phys. C **14**, 2785 (1981).
[62] T. Moriya, Prog. Theor. Phys. **28**, 371 (1962).
[63] S. Sachdev, Phys. Rev. B **50**, 13006 (1994).
[64] J. Steinberg, N. P. Armitage, F. H. L. Essler, and S. Sachdev, Phys. Rev. B **99**, 035156 (2019).
[65] A. W. Sandvik, Phys. Rev. B **52**, R9831 (1995).
[66] O. A. Starykh, A. W. Sandvik, and R. R. P. Singh, Phys. Rev. B **55**, 14953 (1997).
[67] M. Dupont, S. Capponi, and N. Laflorencie, Phys. Rev. B **94**, 144409 (2016).
[68] E. Coira, P. Barmettler, T. Giamarchi, and C. Kollath, Phys. Rev. B **94**, 144408 (2016).
[69] S. Capponi, M. Dupont, A. W. Sandvik, and P. Sengupta, Phys. Rev. B **100**, 094411 (2019).
[70] X. Wang, K. Hallberg, and F. Naef, in *Density-Matrix Renormalization* (Springer, Berlin, Heidelberg, 1999), pp. 173–194.
[71] J. Sirker and A. Klümper, Phys. Rev. B **71**, 241101(R) (2005).
[72] J. Sirker, Phys. Rev. B **73**, 224424 (2006).
[73] T. Barthel, U. Schollwöck, and S. R. White, Phys. Rev. B **79**, 245101 (2009).
[74] C. Karrasch, J. H. Bardarson, and J. E. Moore, Phys. Rev. Lett. **108**, 227206 (2012).
[75] T. Mutou, N. Shibata, and K. Ueda, Phys. Rev. Lett. **81**, 4939 (1998).

[76] F. Naef, X. Wang, X. Zotos, and W. von der Linden, Phys. Rev. B **60**, 359 (1999).
[77] A. W. Sandvik, Phys. Rev. E **94**, 063308 (2016).
[78] H. Shao, Y. Q. Qin, S. Capponi, S. Chesi, Z. Y. Meng, and A. W. Sandvik, Phys. Rev. X **7**, 041072 (2017).
[79] J. W. Britton, B. C. Sawyer, A. C. Keith, C. C. Wang, J. K. Freericks, H. Uys, M. J. Biercuk, and J. J. Bollinger, Nature (London) **484**, 489 (2012).
[80] P. Richerme, Z. X. Gong, A. Lee, C. Senko, J. Smith, M. Foss-Feig, S. Michalakis, A. V. Gorshkov, and C. Monroe, Nature (London) **511**, 198 (2014).
[81] J. G. Bohnet, B. C. Sawyer, J. W. Britton, M. L. Wall, A. M. Rey, M. Foss-feig, and J. J. Bollinger, Science **352**, 1297 (2016).
[82] J. Zeiher, J. Y. Choi, A. Rubio-Abadal, T. Pohl, R. van Bijnen, I. Bloch, and C. Gross, Phys. Rev. X **7**, 041063 (2017).
[83] P. W. Anderson and G. Yuval, J. Phys. C **4**, 607 (1971).
[84] J. M. Kosterlitz and D. J. Thouless, J. Phys. C **6**, 1181 (1973).
[85] K. Fukui and S. Todo, J. Comput. Phys. **228**, 2629 (2009).
[86] S. Todo, Activity Report 2017 of Supercomputer Center, Institute for Solid State Physics, the University of Tokyo, Tokyo (2017).
[87] H. W. J. Blöte and Y. Deng, Phys. Rev. E **66**, 066110 (2002).
[88] A. W. Kinross, M. Fu, T. J. Munsie, H. A. Dabkowska, G. M. Luke, S. Sachdev, and T. Imai, Phys. Rev. X **4**, 031008 (2014).
[89] J. Yoshitake, J. Nasu, and Y. Motome, Phys. Rev. Lett. **117**, 157203 (2016).
[90] N. Janša, A. Zorko, M. Gomilšek, M. Pregelj, K. W. Krämer, D. Biner, A. Biffin, C. Rüegg, and M. Klanjšek, Nat. Phys. **14**, 786 (2018).
[91] G. K. L. Chan, A. Keselman, N. Nakatani, Z. Li, and S. R. White, J. Chem. Phys. **145**, 014102 (2016).
[92] E. M. Stoudenmire and S. R. White, Phys. Rev. Lett. **119**, 046401 (2017).
[93] C. Hubig, I. P. McCulloch, and U. Schollwöck, Phys. Rev. B **95**, 035129 (2017).
[94] T. Nishino, K. Okunishi, Y. Hieida, N. Maeshima, and Y. Akutsu, Nucl. Phys. **B575**, 504 (2000).
[95] K. Okunishi and T. Nishino, Prog. Theor. Phys. **103**, 541 (2000).
[96] L. Vanderstraeten, B. Vanhecke, and F. Verstraete, Phys. Rev. E **98**, 042145 (2018).
[97] W. Tang *et al.* (to be published).